Martin, T. L., Radecka, A., Sun, L., Simm, T., Dye, D., Perkins, K., Gault, B., Moody, M. P., & Bagot, P. A. J. (2016). Insights into microstructural interfaces in aerospace alloys characterised by atom probe tomography. *Materials Science and Technology*, *32*(3), 232-241. https://doi.org/10.1179/1743284715Y.0000000132

Insights into Microstructural Interfaces in Aerospace Alloys Characterised by Atom Probe Tomography

T.L. Martin[1], A. Radecka[2], Lin Sun[3], Thomas Simm[4], D. Dye[2], K. Perkins[4], B. Gault[1], M.P. Moody[1] and P.A.J. Bagot[1].

[1] Department of Materials, University of Oxford

[2] Department of Materials, Imperial College London

[3] Department of Materials Science & Metallurgy, University of Cambridge

[4] Institute of Structural Materials, University of Swansea

Corresponding author: tomas.martin@materials.ox.ac.uk

Abstract

Atom Probe Tomography (APT) is becoming increasingly applied to understand the relationship between structure and composition of new alloys at the micro- and nano-scale and their physical properties. Here, we use APT datasets from two modern aerospace alloys to highlight the detailed information available from APT analysis, along with potential pitfalls that can affect data interpretation. The interface between two phases in a Ti-6Al-4V alloy is used to illustrate the importance of parameter choice when using proximity histograms or concentration profiles to characterise interfacial chemistry. The higher number density of precipitates and large number of constituent elements in a maraging steel (F1E) present additional challenges such as peak overlaps that vary across the dataset, along with inhomogenous interface chemistries.

Keywords: Aerospace, Atom Probe Tomography, alloys, precipitation, interface chemistry, phase partitioning, data analysis, microstructural characterisation

1. Introduction

Detailed characterisation of the atomic architecture of engineering materials is of critical importance for improving their functional and structural properties. For this, atom probe tomography (APT) provides a unique insight into the 3D chemical distributions at a scale that most current electron microscopes cannot routinely achieve.[1] A key strength of APT is the identification of specific interfaces and characterisation of their chemistry, for example, precipitate-matrix interfaces, grain boundaries, or surface oxide-metal interfaces.

An example where such detailed interfacial analyses are playing a vital and rapidly expanding role in is the development of the next generation of aerospace alloys.[2] To fully optimise the alloy performance, understanding the interactions between different elements at the atomic-level is imperative. Even slight changes in overall chemical composition or heat treatment can have a dramatic influence on the structure and composition of precipitates, phases and grain boundaries, which in turn control the material properties. Few other techniques have the

combined spatial resolution and chemical sensitivity to correlate subtle changes in microstructure to this behaviour. In parallel, APT is also underpinning improved understanding of how current generation aerospace alloys perform under the environmental conditions experienced in service.

Standardised specimen preparation techniques, improved instrumentation and straight-forward software for APT reconstruction, visualisation and analysis,[1,3,4] have made APT a routine tool to understand complicated microstructures such as those found in aerospace alloys. However, the correct application of the various analysis methods on offer is non-trivial, in particular when analysing compositional changes at material interfaces. The aim of the present article is to present two examples of APT analyses on aerospace alloys, along with reviewing some potential problems and missteps in the analysis that can have important ramifications for the accuracy of data interpretation.

The two classes of aerospace alloys explored in this paper are a titanium alloy (Ti 6-4) and a maraging steel (F1E). Titanium-based alloys are extensively used for structural components in aircraft frames, engine fan blades and their casings due to their high specific strength, damage tolerance and good corrosion resistance.[5–7] The ratio of the α, β phases, as well as the presence of unwanted ω and Ti_3Al phases, play a key role in controlling the mechanical and thermal properties of these alloys.[8–11] Characterising and controlling the distribution of these phases as well as the roles of interstitial species such as oxygen in Ti 6-4 by APT continues to help better understand their role on the critical mechanical properties.[12,13]

Along with developments on novel Ti alloys, work continues on refining steel alloys for high stress environments in gas-turbine engines. For instance, F1E is a new maraging steel alloy designed to act as a continuous element all the way along a central shaft in future engines.[14] The proposed reduction in engine diameter will lead to weight reductions and greater thermal and propulsion efficiency, but also increase the operational temperature and stresses. The latter both require careful design of the microstructure to prevent creep degradation. These maraging steels have several competing types of precipitates that determine their mechanical properties, the smallest of which are difficult to characterise using any other technique than APT.[15–17]

Although APT is an incredibly powerful tool to analyse the complex microstructures that modern alloys rely on for their advanced physical properties, the interpretation of the data produced is not always straightforward, and attention has begun to turn towards addressing this in the literature[18,19]. Datasets can consist of tens or even hundreds of millions of atoms, and choosing the correct parameters for analysing interfacial chemical profiles is vital to ensure small changes in chemistry between phases are accurately characterised. In addition, the mass spectra from modern alloys include contributions from multiple elements, and individual isotopes of these may overlap with each other. A further complication arises when a peak identified in the mass spectrum containing overlapping isotopes is present in two different phases; the elements contributing to the overlap may in some cases differ between each phase.

This paper aims to identify several such pitfalls that can commonly occur in aerospace alloys, with the intention of improving understanding of the use of interfacial analysis in APT.

2. Materials and Methods

The titanium alloy characterised in this study was Ti 6-4, containing 6 wt.% Al and 4 wt.% V, with around 1800ppm O expected. A section of uni-directional (UD) rolled plate Ti 6-4 as manufactured by TIMET was supplied by Rolls-Royce Plc. This was prepared by double Vacuum Arc Remelting (VAR), followed by beta forging and subsequent alpha beta forging. The samples were then alpha beta rolled to produce plate. Afterward the material was creep flattened, machined, pickled and inspected before a heat treatment at 550°C for 28 days.

The second alloy studied was a maraging steel, F1E. This alloy contains (all wt.%) 68.1% Fe, 6.99%Ni, 9.90% Cr, 8.02% Co, 2.75% Mo, 2.43% W and 1.80% Al. The alloy was vacuum induction melted by Tata RD&T Swindon technology centre into 60kg ingots and then hot forged into 50mm x 50mm square bars. The forged bars were solution heat treated in vacuum at 1200 ˚C for 48 hours followed by an Argon gas quench. Following this, the material had had a two-step heat treatment - firstly an 825 ˚C austenisation for 2 hours followed by ageing at 560 ˚C for 5 hours.

All APT experiments were performed using a Cameca LEAP 3000X HR commercial atom probe instrument. Specimens were run in laser-pulsing mode, at a base temperature in the 40–55K range, a laser pulse energy of 0.2-0.4nJ and a pulse repetition rate of 200 kHz at a wavelength of 535nm.

Specimens were prepared via Focused Ion Beam (FIB) using the liftout and annular milling method described by Thompson and co-workers.[20–22] FEI Helios NanoLab Dual Beam and Zeiss NVision FIB instruments were used to produce needle-shaped specimens with tip diameters of approximately 50nm suitable for APT analysis.

3. Results and Discussion

3.1 Ti 6-4 alloy – example of a simple two phase boundary in APT

Firstly we examine the Ti 6-4 alloy following 28 days heat treatment, which has a relatively simple two-phase microstructure. Approximately half of all titanium used in aerospace is in the form of Ti 6-4,[5] and controlling the ratio and composition of the α- and β-phases is important to the resulting properties of the alloy. Figure 1 shows an SEM photomicrograph of the Ti 6-4 microstructure in the specimen studied, showing a majority of equiaxed α grains with lighter coloured platelets of β-phase between the α grains.

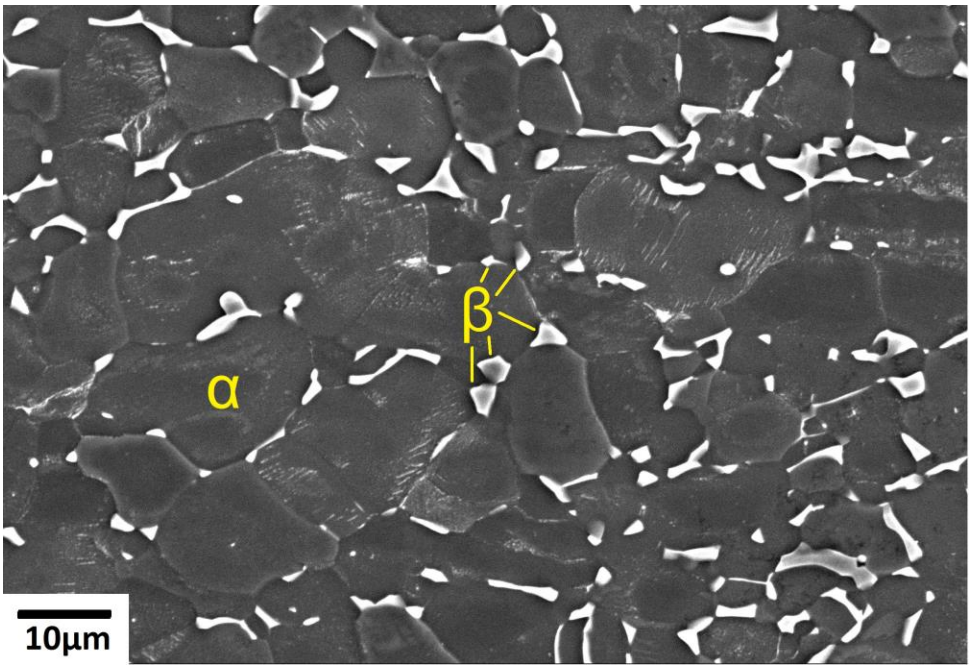

Figure 1: Scanning Electron Micrograph image at 1200x showing the grain structure of Ti 6-4 after 28 days heat treatment at 550°C. The α- and β-phases are labelled.

In Figure 2 a series of atom maps from a single APT reconstruction of a needle specimen of the same Ti 6-4 material are presented. This type of visual representation is the simplest way that APT contributes to the study of these materials. The first atom map in Figure 2(a) shows all of the ions, with each dot representing an atom, and each colour corresponding to a ranged element. Two phases are clearly observed, the associated change in chemistry indicated by the colour change halfway down the specimen.

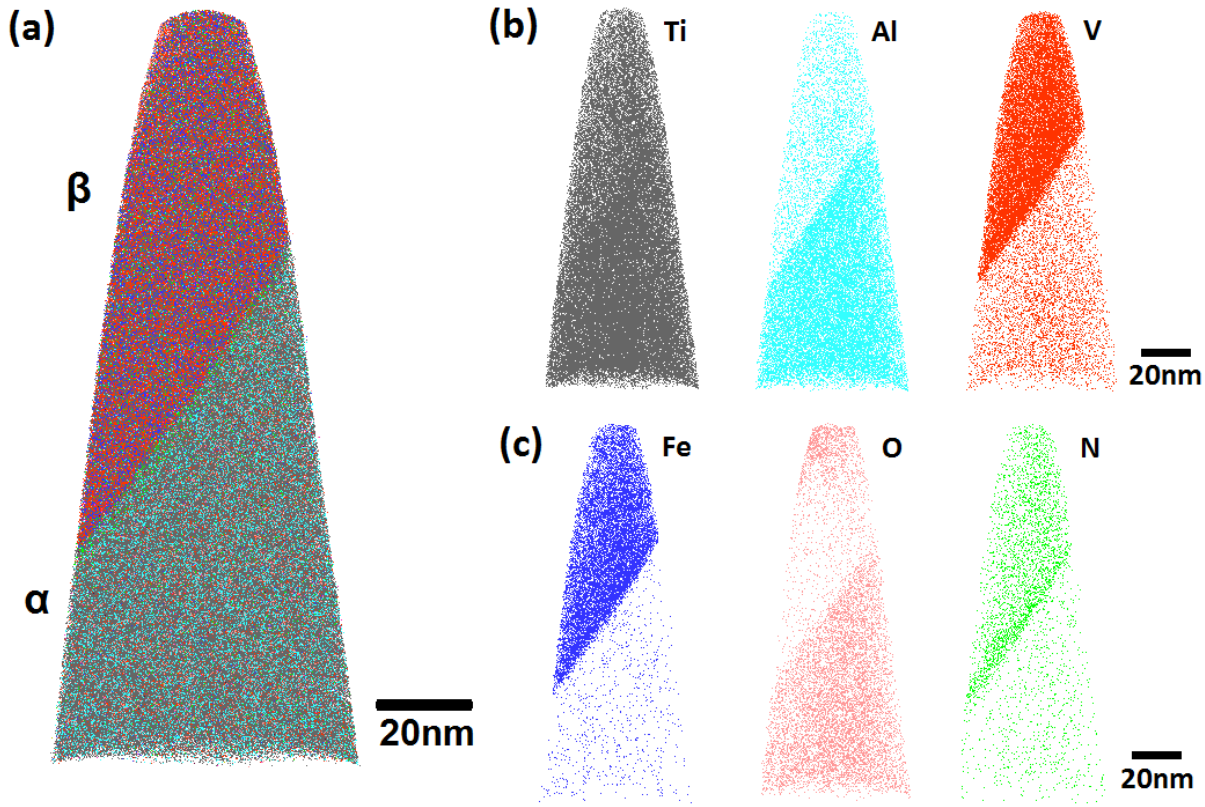

Figure 2: (a) Atom map of Ti 6-4 alloy with beta and alpha regions. (b) Individual atom maps for the principle elements in the alloy - Ti, Al and V. (c) Other minor elements showing significant segregation – Fe, O and N.

In Figure 2(b) and (c), the overall atom map from Figure 2(a) is split into spatially-resolved maps for each element. The number of atoms visualised in each case is limited to no more than 100,000 for ease of comparison. As expected, Al and V segregate in different directions into the two different phases. Thus the upper phase with enriched V and depleted Al can be identified as the edge of a β-phase precipitate, whilst the lower section is the more prevalent α matrix.

For the minor elements, the overall dataset reveals 1.07 at.% Fe, 0.67 at.% O (in the form of TiO complex ions) and just 0.23 at.% N. Despite the low percentages of these elements, the APT data clearly shows marked segregation behaviour of the minor species that could be significant to the performance of the alloy – Fe and N are clearly segregated to the β-phase, whilst O is mainly found within the α-phase, aside from a small amount at the top of the tip which can be ascribed to surface oxidation. Precise measurements regarding the overall composition of the two phases can be extracted from this APT data. By separating the dataset into the α- and β-phases, the respective compositions are shown in Table 1. The most notable feature of this is just how much higher the concentration of V in the β-phase is, compared to the nominal composition and to the amount in the α-phase. Considering from Figure 1 that the β volume fraction is relatively low, this segregation can be understood more clearly. The possibility that

the N content is higher in the β-phase rather than the α-phase is also intriguing, as traditionally nitrogen has been considered to favour the α-phase.[23]

Element	Nominal bulk composition (wt.%)	α-phase composition (wt.%)	β-phase composition (wt.%)
Ti	87.6%	90.4%	66.2%
Al	5.5-6.75%	5.72%	1.42%
V	3.5-4.5%	3.18%	27.6%
O	<=0.2%	0.29%	0.11%
Fe	<=0.4%	0.06%	3.91%
N	=0.05%	0.04%	0.14%

Table 1: Nominal composition of the Ti 6-4 alloy, together with the α- and β-phase compositions taken from the atom probe dataset. The atom probe data has been converted to weight % for ease of comparison.

3.2 Parameter selection in interfacial chemistry analysis

As well as providing information on the composition of phases in a material, APT can also provide high-resolution information about the change in composition *across* the interface between two phases, grains or between precipitates and matrix regions. As such interfaces often play a significant role in how the material performs under stress and corrosive conditions, the insights that APT can provide are of significant interest in the study of new alloy microstructures and in understanding damage such as stress-corrosion cracking. [24,25]

There are a number of different ways to analyse the composition across interfacial regions between phases or precipitates in an atom probe reconstruction, but there is no standard protocol for how to use them.[26,27] For instance, a one-dimensional concentration profile plotting the local composition across a cylindrical or cuboidal region of interest positioned running through the interface is simple to administer and adjust, but is less accurate across interfaces that are non-planar. An alternative is to use an iso-concentration surface (isosurface), highlighting regions where the concentration of a desired element is above a certain concentration, and following this by plotting a proximity histogram (proxigram) to give a concentration profile as a function of distance either side of the interface defined by the isosurface.[28,29]

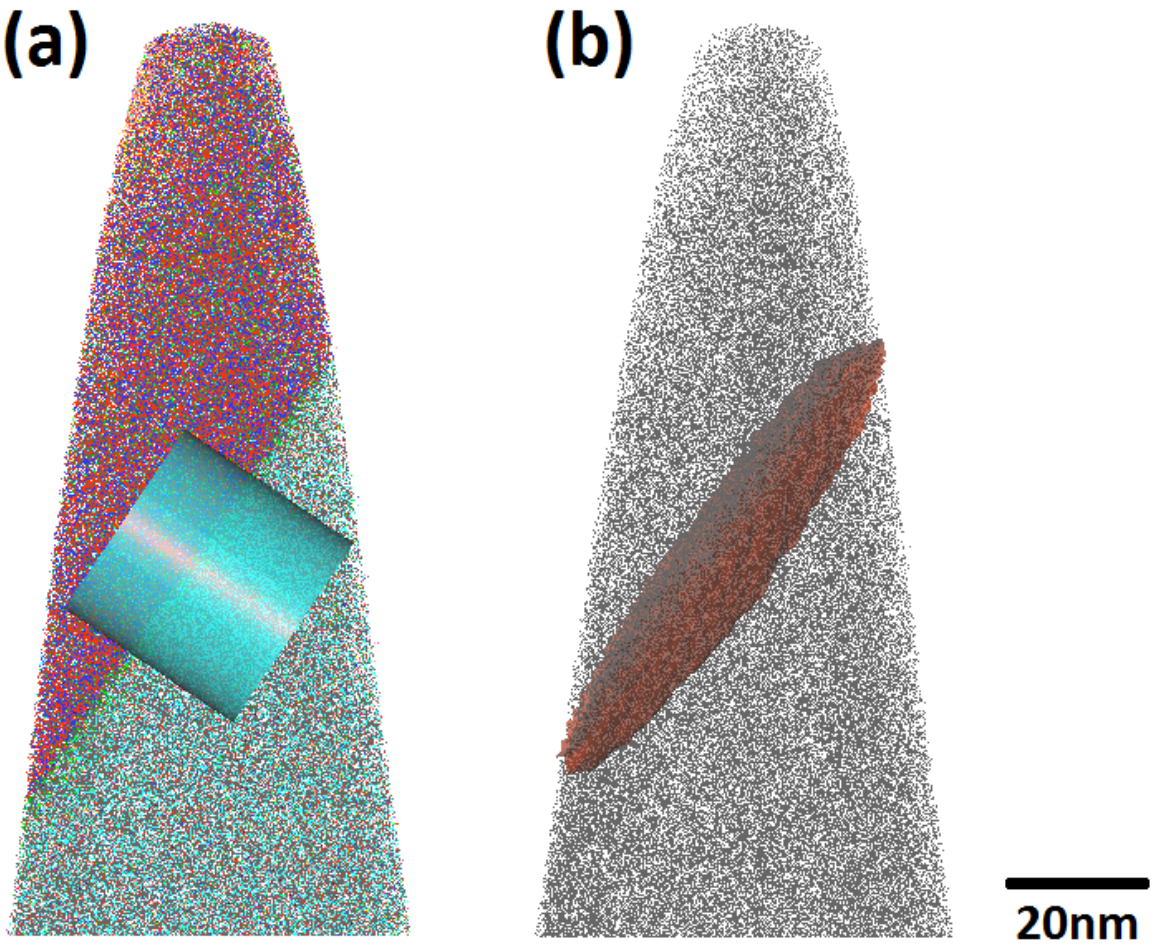

Figure 3: Illustration of the two primary interface analysis tools in APT. (a) the cylindrical region of interest used to create a one-dimensional concentration profile and (b) a 12.7 at% V isosurface used to create a proximity histogram.

Figure 3 shows examples of these different ways of getting compositional information across an interface between different phases. Figure 3(a) shows a cylindrical region-of-interest (ROI) placed across the interface between the α- and β-phases. Once the ROI is appropriately sized, located and oriented it can be used to create a 1D concentration profile down the length (z-axis) of the cylinder, as shown in Figure 4.

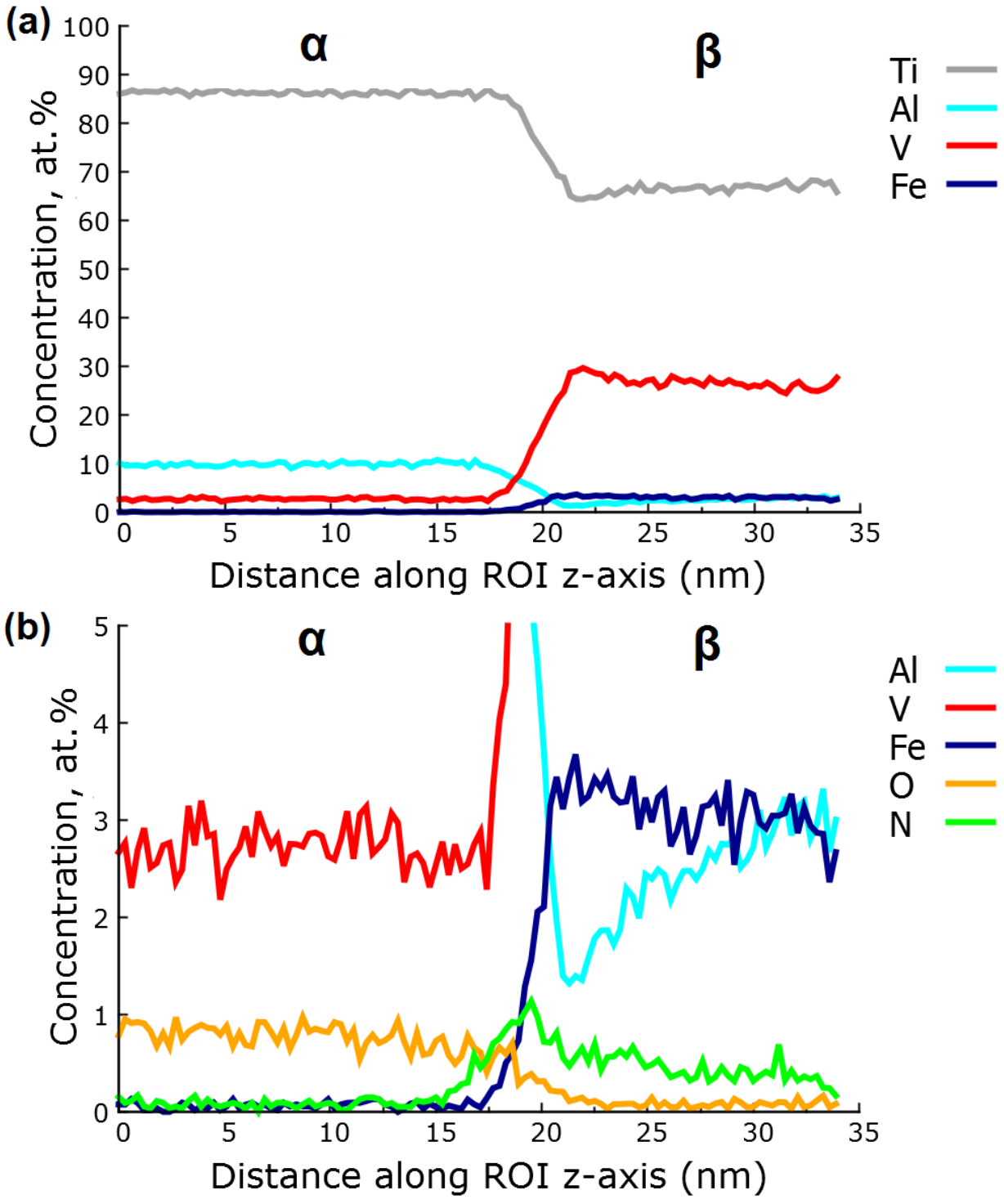

Figure 4: 1 dimensional concentration profiles across the z-axis of the cylindrical region of interest shown in Figure 3. (b) is zoomed 20x to show minor elements.

Figure 4 shows a one-dimensional concentration profile along the z-axis of the cylindrical region of interest shown in Figure 3(a). This method provides a quantitative analysis of the chemical

partitioning to complement the preliminary conclusions provided by the atom maps in Figure 2. The α-phase consists of approximately 87 at.% Ti with 10 at.% Al and 2.5 at.% V, with oxygen present at around 0.85 at.%. In the β-phase, the Ti content falls to around 67 at.%, the Al content drops to approximately 2.9 at.%, whilst the V content increases dramatically to 26 at.%, with a slightly higher concentration at the boundary between the two phases. Fe increases to around 3 at.% in the beta phase from a negligible concentration in the α-phase, whilst N content increases and O content falls significantly in the β-phase, with a possible segregation of N observable at the boundary between the two phases.

The 1D concentration profile is a powerful tool to assess compositional changes between phases and thin layers of differing composition. However, choosing the right parameters that underpin the application of this analysis is critical to create an accurate description of the compositional change. Here we illustrate the importance of optimising the parameter selection.

To show the parameter dependence on accurate 1D concentration profiles, we generated artificial atom probe datasets using a MATLAB script that generates a list of atomic positions, where all atoms sit on a face-centered cubic lattice with a fixed lattice parameter (here 0.357 nm)[30,31]. Each atom in the list is then attributed a mass-to-charge ratio. A different mass-to-charge ratio can be attributed based upon a set of criteria, i.e. their location with respect to an interface, allowing the introduction of different atomic species within the volume. For the purposes of this study further randomisation of the atomic position to account for the spatial resolution and detector efficiency were not implemented, with every atom retained and located on a perfect lattice.

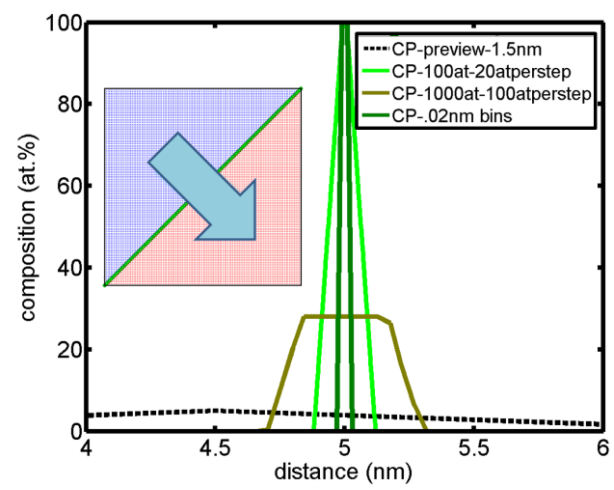

Figure 5: 1D concentration profiles through a computationally simulated A-B interface,with a monolayer of C lying at the interface. Each curve uses a different set of parameters for the concentration profile, indicating the importance of correct implementation of the 1D profile tool.

The dataset was generated with an interface at 45 degrees between elements A (in blue) and B (in red), as shown inset to Figure 5. At the interface sits a monolayer of C (in green). A 5x5x10 nm cuboidal region-of-interest has been positioned in the centre of the dataset and aligned with the long axis normal to the interface. Making use of the standard commercial APT software (Cameca IVAS 3.6.6), four different profiles were computed using different binning parameters, which are compared in the main part of Figure 5. The initial profile, as demonstrated by the black dotted line in Figure 5 and called *Preview* in IVAS, makes use of a very coarse binning (1.5 nm) and the presence of the monolayer of C is effectively not detected.

Figure 5 also indicates that if smoothing is applied to the profile, it must be undertaken with care. Whilst all three other curves pick up the increase in C concentration, the dark green profile, which uses a fixed sample count of 1000 atoms and 100 atoms per step, broadens the distribution of the C layer unrealistically, with a composition of approx. 28% and an intermixing of A and B. The other two profiles, in light green and brown, use step sizes of 20nm and 0.2nm respectively, and both correctly identify the complete C monolayer, with the composition reaching 100% over a distance corresponding to approximately an interplanar spacing. Although this issue is well known to more experienced atom probe users, the common mistake of incorrect parameter choices can lead to composition profiles that appear to either be overly smoothed or with a bin size too large to reflect the actual changes in composition at the scale of the features of interest.

An alternative to the 1D concentration profile is to use a proximity histogram, where the interface is mapped by an iso-concentration surface for an appropriate element, followed by the plotting of the localised composition as a function of increasing perpendicular distance away from both sides of the interface.[28,29] This proximity histogram has the benefit of eliminating the shape of the interface from consideration, and if combined with the correct parameters can result in sharper profiles across the interface than for the 1D concentration profile. The increased area of the interface sampled and hence increased statistics are especially useful when tracking the behaviour of low concentration components across the interface. Figure 3 (b) shows the alternate approach as applied to the Ti- 6-4 specimen. As vanadium is the element that changes concentration most between the two phases, an iso-concentration surface using this element has been created. The level of concentration displayed within the surface can be varied until it best highlights the interface. In this case a 12.7% V isosurface has been selected and used to create the proxigram shown in Figure 6.

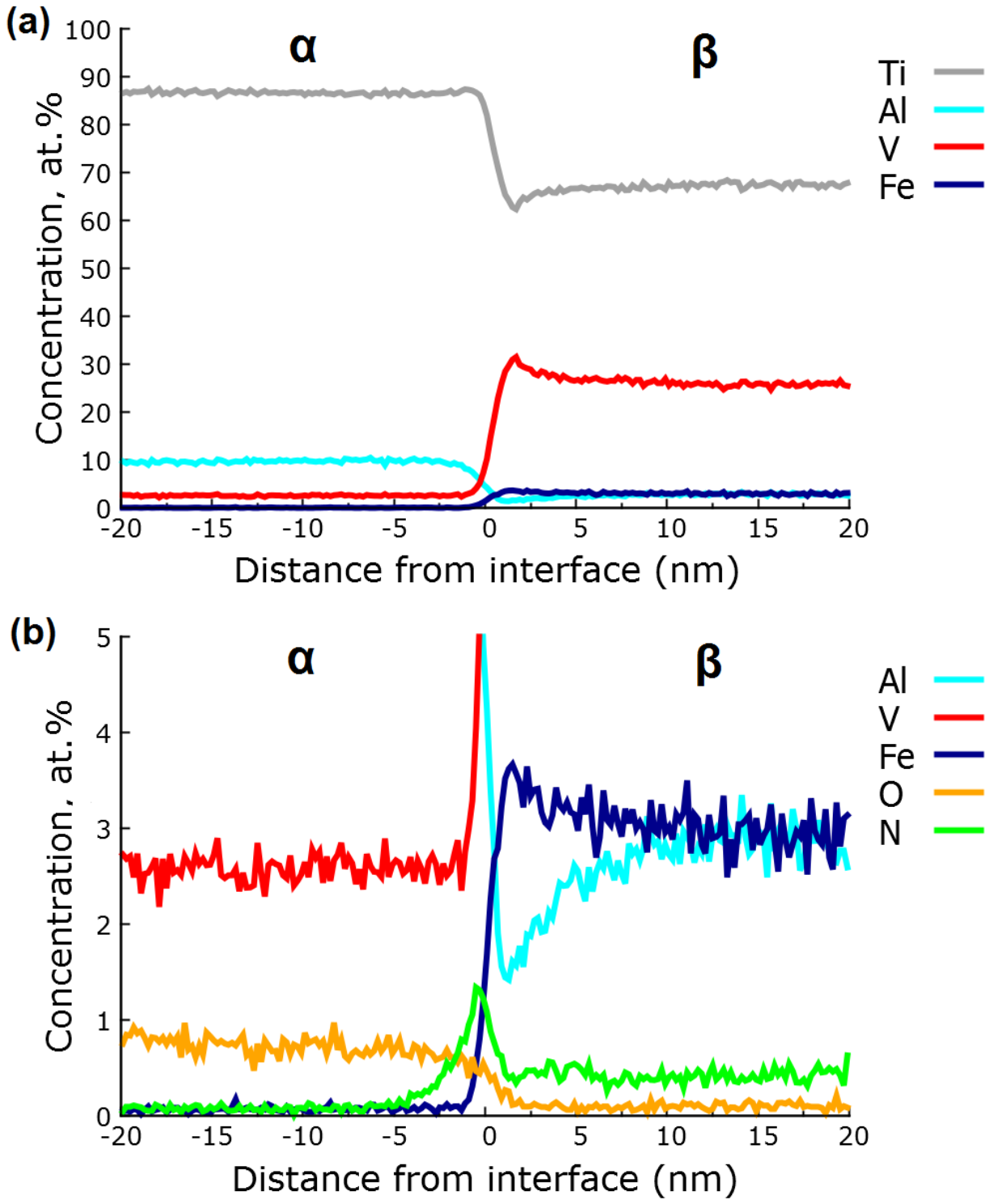

Figure 6: Proxigram of Ti 6-4 sample through the interface highlighted in Figure 3 (b). (a) shows the full range of concentrations whilst (b) zooms in x20 to show elements with less than 5 at.% concentration.

Figure 6(a) shows the proxigram across 20nm of the interface between the α- and β-phases displayed in Figure 3(b) for all elements, whilst Figure 6(b) is magnified by 20x to focus on the minor elements segregating to both phases and the boundary. As with the 1D concentration profile we see a shift from a high titanium and aluminium region in the α-phase, to much higher vanadium and iron content within the β-phase, with accompanying change in minor elements such as O and N, which segregate in opposite directions. Compared to the one-dimensional profile shown in Figure 4, the proxigram in Figure 6 has a sharper interface, and the spike of N at the boundary is much more easily distinguished.

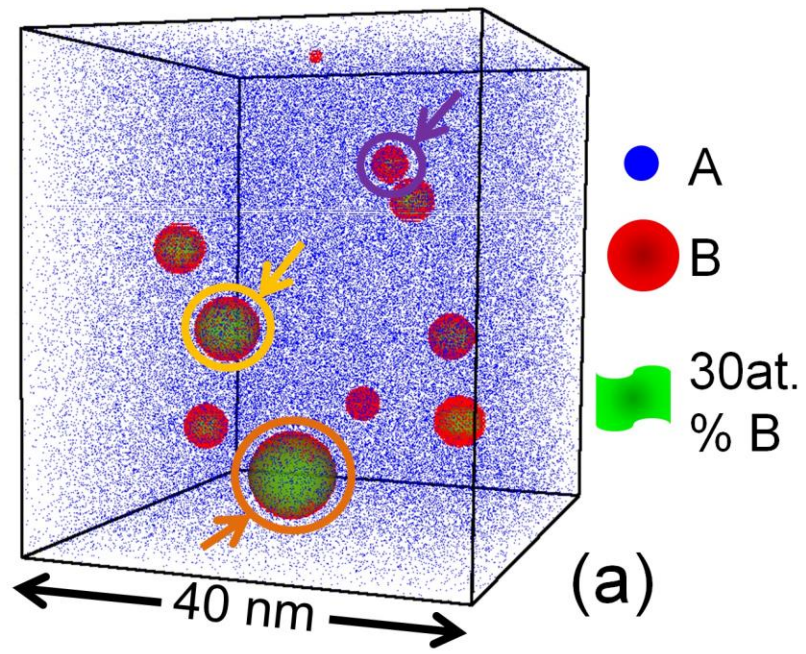
A
B
30at.
% B
40 nm
(a)

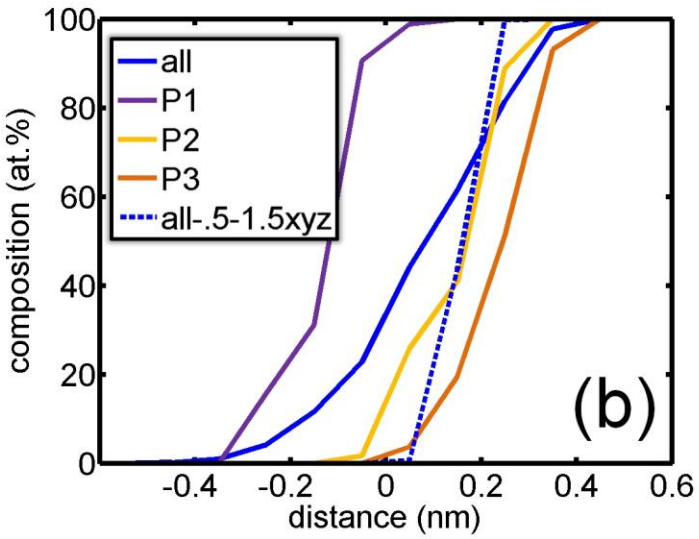
all
P1
P2
P3
all-.5-1.5xyz
composition (at.%)
distance (nm)
(b)

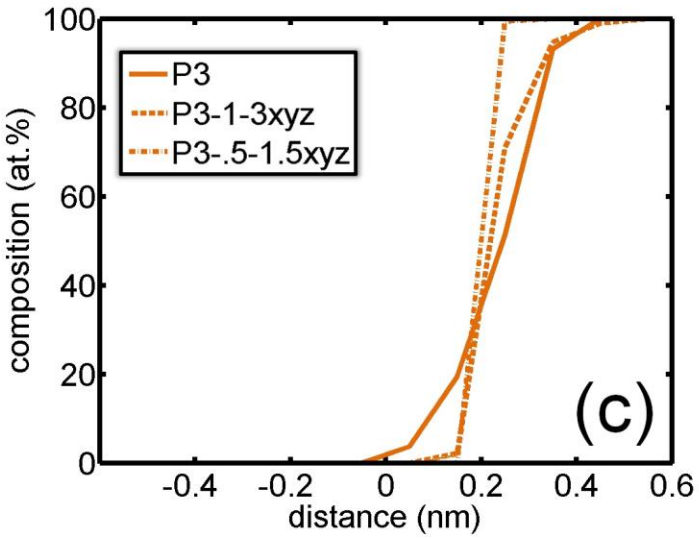
P3
P3-1-3xyz
P3-.5-1.5xyz
composition (at.%)
distance (nm)
(c)

Figure 7: (a) simulated dataset with 10 particles of species B (red spheres) in a matrix of species A (blue dots). A 30 at.% B isoconcentration surface (green) highlights particles. (b) Proxigram for three different particle sizes, as well as an average across the three particles, showing the shift in interface position. (c) Proxigram of B for different grid parameters of the largest of the three particles circled in (a).

The correct use of proxigrams for interfacial analysis can still present challenges, as proxigrams are also parameter-dependent. Proximity histograms are computed from isoconcentration surfaces that are placed on a grid superimposed to the dataset and smoothed by a delocalisation process.[28,29] To highlight the issues associated with such an approach, we have again generated a simulated APT dataset using similar parameters to the method used for the concentration profile described above. In this case, as shown in Figure 7(a), the simulated dataset consists of 10 particles of pure element B, varying in size from 0.55nm to 3.55nm, within a matrix of element A. A single 30% B isoconcentration surface highlights the edge of these particles[32], and has been used to create proxigrams for each individual particle, as well as proxigram profiles averaged across all of the particles.

To investigate the influence of parameter selection, initially the current default parameters of the software were implemented, which corresponds to an xyz grid of 1 x 1 x 1 nm and delocalisation of 3 x 3 x 1.5 nm. Three particles with radii of approximately 3.55, 2.55 and 1.55 nm were selected, as circled in orange, yellow and purple in Figure 7(a), and labelled as P1, P2 and P3 in Figure 7(b). Because the three particles are of different sizes but use the same grid, the relative positions of the interfaces for P1, P2 and P3 on the proxigram in Figure 7(b) shifts the position of the interface as defined by the isoconcentration surface so that it is not always at zero.

A significant issue arises when a single proxigram is computed to describe an average interface for particles in the system in general. This is an option provided by the software and one frequently implemented. Effectively, it is equivalent to summing individual proxigrams for each different sized particle, and in this case results in the artificially broad interface labelled ‘all’ in Figure 7(b). This profile could be erroneously interpreted as an intermixing between the precipitates and the matrix, but it is simply an artefact linked to its computation across particles of different sizes.

Additionally, to show the effect of the grid parameters, two additional proxigrams were computed for P3, the first with an xyz grid size of 1 x 1 x 1 nm and an isotropic delocalisation of 3 nm and the second with a different grid size of 0.5 x 0.5 x 0.5 nm and an isotropic delocalisation of 1.5nm. Figure 7(c) shows how the gradient of the proxigram for the ‘P3’ and ‘all’ profiles depends on the grid size and delocalisation parameters in Figure 7(c), and it is clear using the higher delocalisation in particular results in an overly broad interface that leads to erroneous profiles and compositional analysis.

3.3. F1E Maraging Steel – An example of more complex microstructure in APT

In alloys containing more elements, like the maraging steel F1E, the microstructures can be more complicated, and the relatively straightforward analysis shown for the Ti 6-4 interface is not sufficient to obtain the correct interface chemistry, even if the parameters used for the 1D concentration profile or proxigram are correct. Figure 8 shows a typical atom map for F1E after austenisation at 825°C for one hour and ageing at 560°C for five hours. A high number density of precipitates within the atom probe dataset are visible. These precipitates are primarily of two types – NiAl β-phase precipitates around 5nm in size, as well as larger Laves phase precipitates rich in Mo, W and Cr. The β-phase precipitates are vital to the structural properties of the alloy as they act as barriers to dislocation migration, but due to their size and the similar contrast of Ni, Al and Fe in an electron microscope, they are difficult to see in TEM. APT is therefore one of the few techniques able to examine these important features.

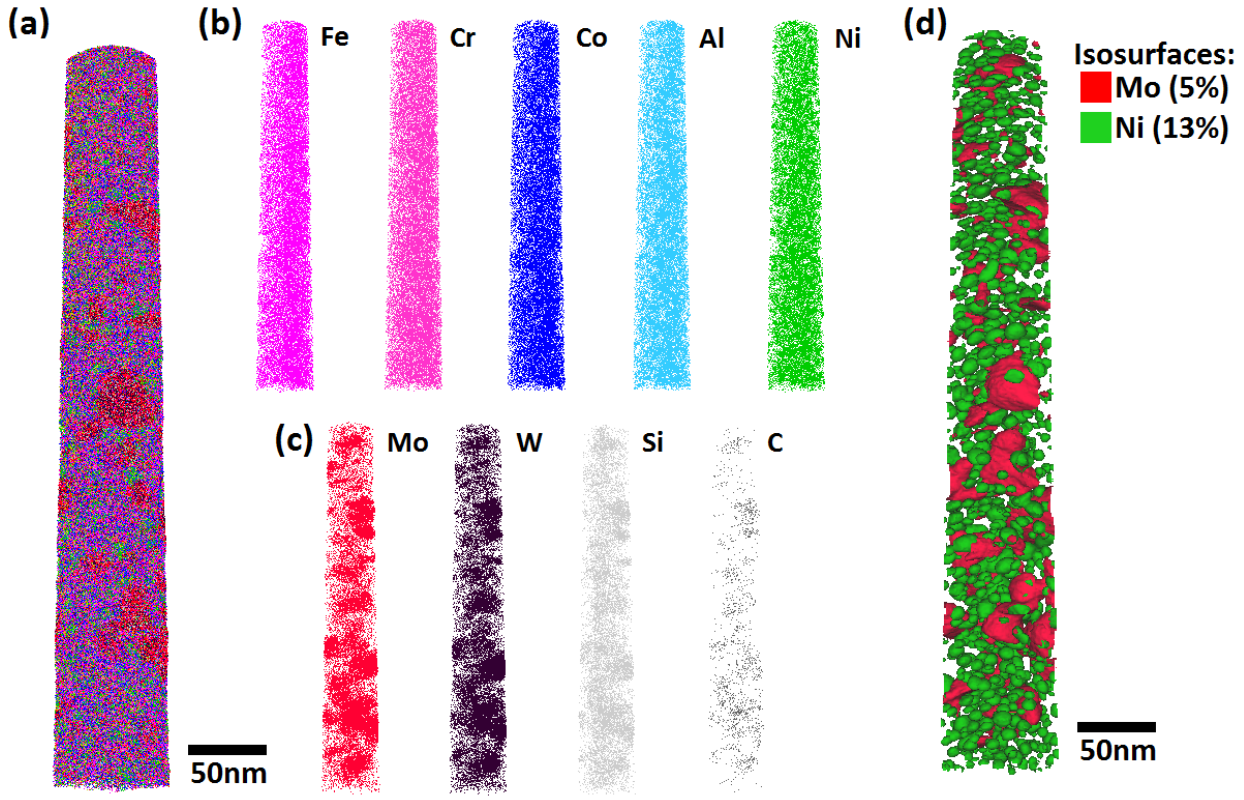

Figure 8: (a) atom map of an aged F1E steel, (b) individual atom maps for the matrix and NiAl β-phase precipitates forming elements, (c) Laves phase forming elements and (d) isoconcentration surfaces of 5% Mo indicating the position of MoW-rich Laves phase (red) and 13% Ni indicating the position of smaller NiAl-rich β-phase precipitates (green).

Due to the large number of precipitates in this analysis volume, a simple proximity histogram approach is inappropriate when studying the chemistry of boundaries, and a more statistical approach comparing the composition of the precipitates to their size must be performed.

3.4. Variation in the identity of a mass/charge peak across an interface

However, as with the previous two materials, there are some issues that complicate the analysis of this dataset. The first is a significant overlap in the APT mass-to-charge-state ratio spectra for F1E between $^{54}Fe^{2+}$ and $^{27}Al^{+}$ ion isotopes. In the bulk composition of the material, there is much higher Fe content than Al, however almost all of the Al is present in the β-phase precipitates, where there is comparatively little Fe. This result is that specifying the 27 Da peak in the mass spectrum as either one of these isotopes will yield an incorrect composition on either side of the β-phase-matrix interface.

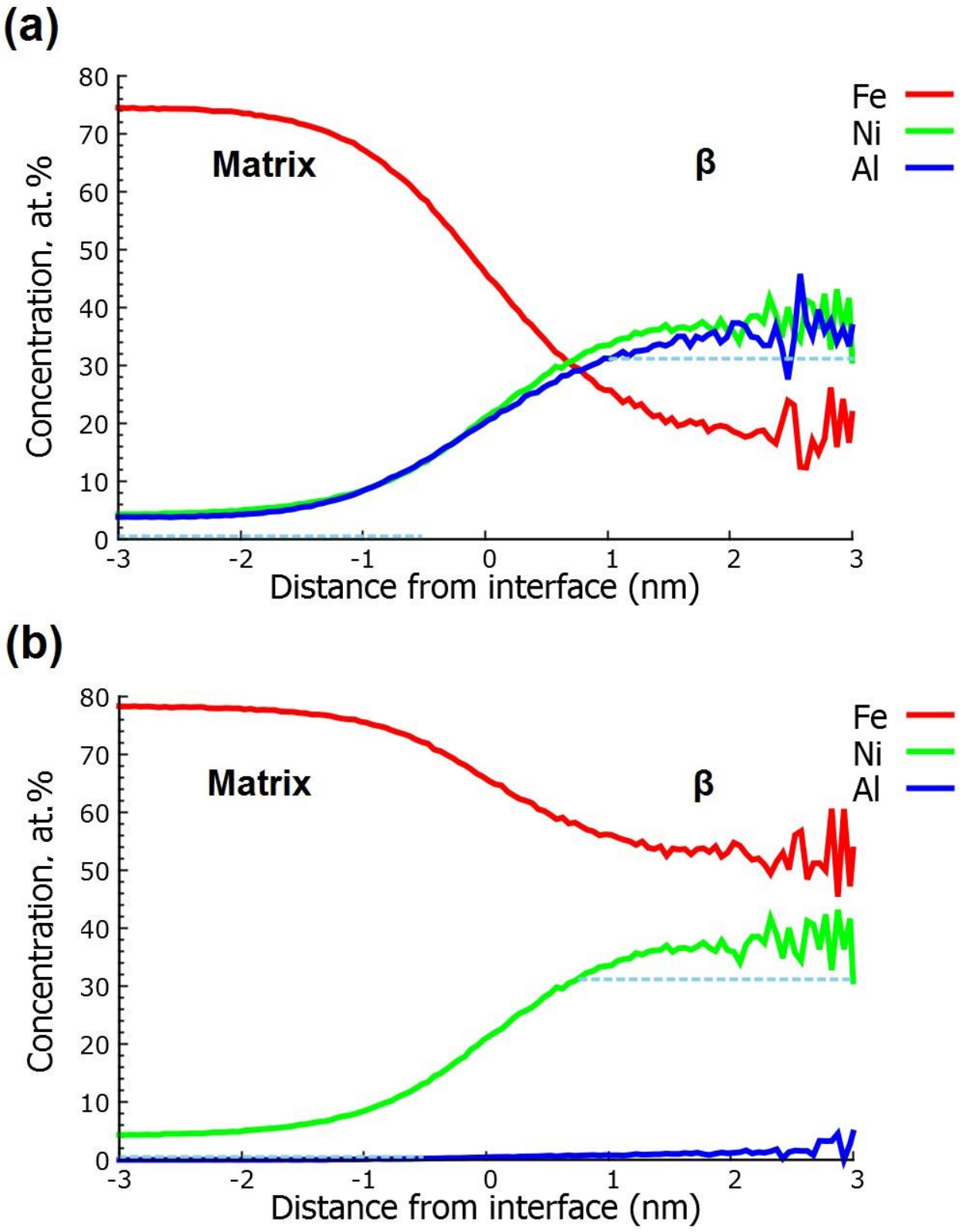

Figure 9 – Proxigrams across the boundary between the aged F1E matrix and several β-phase precipitates of the same size, illustrating the critical importance of ranging to correct

compositional information. In Figure 9(a), the 27 Da peak is ranged as Al, whilst Figure 9(b) shows the same data but with the 27 Da peak ranged as Fe. The dashed light blue line on each figure shows the computationally predicted Al concentration in the matrix and β-phase precipitate respectively.

Figure 9 graphically illustrates this point by showing proxigrams across the boundaries of several β-phase precipitates of a similar size (to avoid the issue with smoothing discussed earlier). The dashed line shows the expected concentration of Al in both the matrix and β-phase precipitates after the applied heat treatment, as calculated from MatCalc software and the MC_FE_2.009 database. If, as in Figure 9(a), the 27 Da peak is ranged as Al, the composition of the NiAl precipitate (right hand side of graph) is approximately 34 at.%, slightly above the computationally predicted value of 31.1 at.%, the difference due to the relatively small fraction of the 27 Da peak belonging to Fe. However, in the matrix the Al content of 7 at.% is much higher than the 0.5 at.% level predicted computationally, as the vast majority of the ions in the matrix with a mass/charge ratio of 27 Da are Fe.

When the 27 Da peak is ranged as Fe, as in Figure 9(b), the Al composition in the bulk is too low at 0.2 at.%, and only rises to around 2% in the NiAl precipitates, which is obviously incorrect. Although a peak deconvolution algorithm in the IVAS software can be applied to estimate the relative contributions of Al or Fe to 27 Da, this is generally applied to the bulk composition measurement, but not to discriminate chemical identity on an atom-by-atom basis. Hence it does not account for partitioning of certain species to secondary phases, and in particular the concentration profile at the interface between two different regions of the microstructure. Thus in this case the accuracy of the proxigram analysis remains limited.

Other researchers have suggested a location-specific chemical ranging to deal with this issue. For example London *et al.* developed a computational approach to isolate localised spatial regions of the data (in that case these were regions identified as solute clusters or precipitates).[33] In that work, the mass-to-charge-state spectrum due to ions solely in each region was isolated, and the peak deconvolution was applied. Hence the peak deconvolution process was correlated to the local chemistry of a region of the microstructure, greatly increasing the accuracy of the compositional analysis within each volume.

Alternatively, in the analysis of the F1E steel in Figure 8, the precipitate and matrix regions could simply be isolated and separated into two datasets, then the mass spectrum ranged respectively for independent analysis of their compositions. However, the interfacial composition profile remains problematic, whether examined by 1D concentration profile or proxigram. Given sufficient statistics, such as in the local-ranging method described above, the mass spectrum from each of the bin of the proxigram could be analysed individually and contributions to the 27 Da peak deconvolved. However this approach has yet to be robustly demonstrated. Smaller bins in the proxigram analysis increase spatial accuracy, however the trade-off is the requirement of sufficient ions to be contained within each bin to be able to make an accurate deconvolution of each point. Choosing wider bin sizes for improved

deconvolution statistics risks smoothing the profile to the point that the data is obscured. When this occurs in a dataset, this is a difficult problem to wholly address, and requires continued development of new location-specific ranging tools.

3.5. Analysis of the interface of a precipitate with inhomogenous neighbouring regions

Analysis of the composition of the Laves phase in the aged F1E maraging steel is also complicated by the fact that whilst the internal composition of the particle is homogenous, the surface content varies widely, both from particle to particle, but also sometimes across the surface of a single particle. As a result, the traditional proximity histogram used for isoconcentration surfaces is not appropriate, as the resulting profile would average regions of the same surface of differing composition. Instead, an ROI-based approach using several 1D concentration profiles must be implemented.

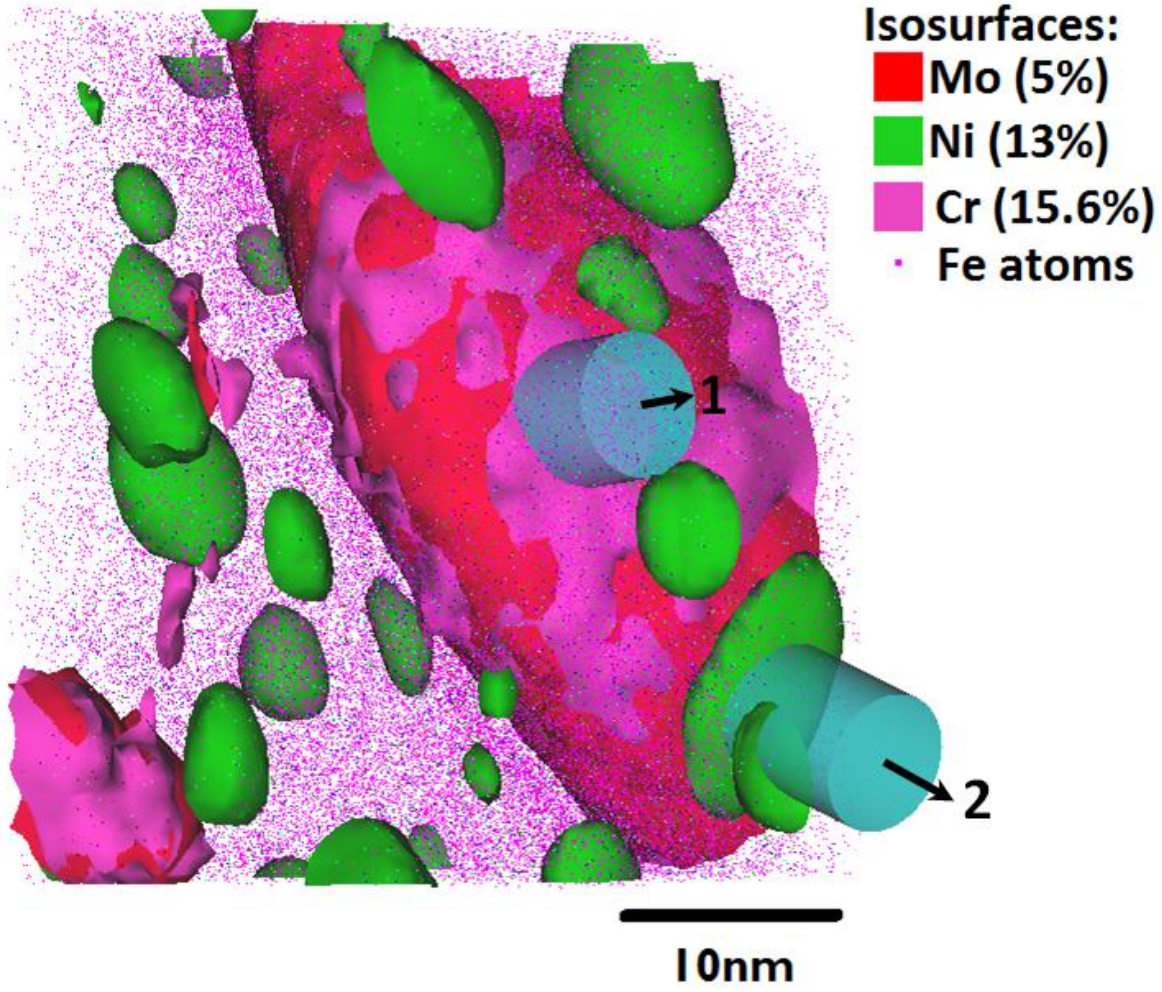

Figure 10: Close up of a Laves phase particle in F1E maraging steel, where several NiAl β-phase precipitates are present close to the interface between the Laves particle and the matrix. Arrows marked 1 and 2 are present to indicate the direction of the cylinder ROIs used for the two one-dimensional concentration profiles shown in Figure 12(a) and (b) respectively.

Figure 10 highlights an example Laves phase particle in red, Cr-rich regions in pink and Ni precipitates in green, with a fraction of Fe atoms shown. One dimensional concentration profiles have been used to analyse the composition through ROI cylinders intersecting the Laves-matrix at two different places on the surface of the Laves, as indicated by arrows 1 and 2 on Figure 10. As discussed earlier, getting the correct parameters for this process is important to achieving an accurate composition profile – too low sampling and interesting features are smoothed out, whereas too high sampling means the graph is dominated by noise. In this case, a 3D grid of 1x1x1nm and a delocalisation of 3nm was used, and a fixed sample count of 2000 atoms, with 200 atoms per step, gave the best quality profile.

Figure 11(a) shows a region of the Laves phase where the surface is enriched with Cr, marked as arrow 1 in Figure 10. Although there is also around 15% of Cr in the centre of the Laves phase, at the interface with the matrix this rises to 22%, whilst the level of Mo and W begins to drop to matrix concentrations.

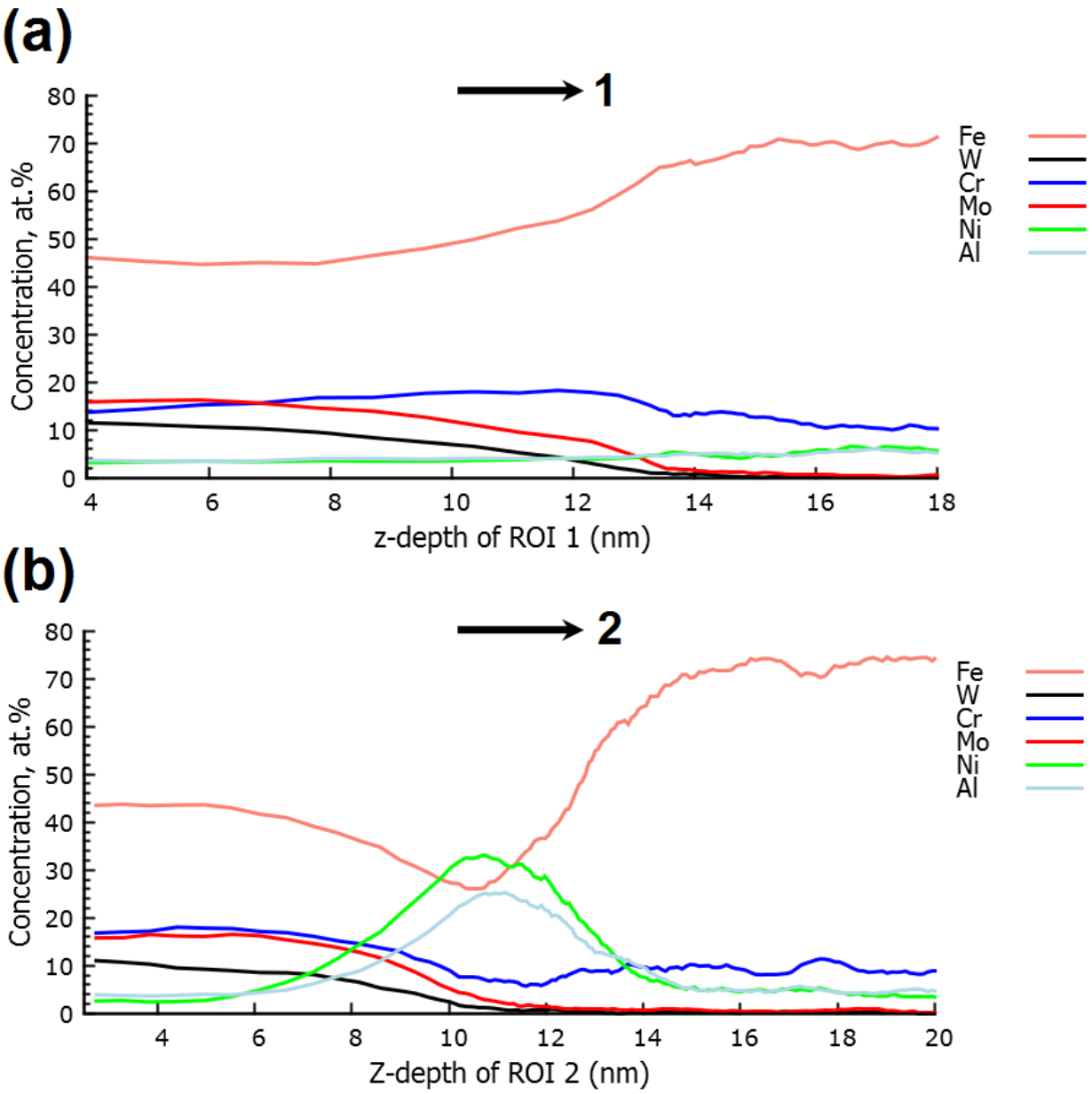

Figure 11 – 1D concentration profile showing the interfacial composition of different areas of the Laves phase precipitate shown in Figure 10. (a) shows a line profile in the direction shown as arrow 1 in Figure 10, whilst (b) shows a line profile in the direction of the arrow marked as 2 in Figure 10. Both profiles use a 1x1x1nm grid with 3nm delocalisation, and a sampling of 1000atoms with 100 atoms per step.

Figure 11(b) shows a region on the surface of the Laves particle, marked as arrow 2 in Figure 10, where there are instead elevated levels of Ni and Al. The second area is similar in composition to the β-NiAl precipitates, but with a flatter morphology adhering to the surface of the Laves. Unlike on the rest of the particle, there is no increase of Cr levels at the interface where the NiAl particle is present. If a proxigram had been used on the entirety of the Laves particle, the

presence of this β-precipitate would have been averaged across the whole surface, producing a inaccurate picture of the localised interfacial composition.

APT datasets of materials of the complexity of this aged F1E maraging steel are of huge benefit to the understanding of the microstructure that drives their mechanical and thermal properties, and to help design alloys that better cope with the stresses experienced in a future gas turbine engines, as well as countless other applications. Without visual inspection of interface surfaces to identify the correct analysis method to employ and careful consideration of the parameter choice and analysis techniques used in the interfacial chemistry, the conclusion of the analysis can be incorrect. As APT becomes a more widely used technique in material science it is vital that such powerful analysis techniques are used to their full potential.

4. Conclusions

Atom Probe Tomography (APT) is of growing importance to understanding the microstructure of new alloys for aerospace applications, as well as the impact of in-service use on their chemistry and microstructure. The atom-by-atom nature of atom probe datasets means that the spatial distribution of elements across interfacial boundaries between grains, phases and precipitates can be mapped to very high resolution.

Although APT is a powerful and increasingly user-friendly technique, the analysis of such interfacial chemistries, whether using one-dimensional concentration profiles or proximity histograms, can present certain challenges. Choosing incorrect parameters for either method can obscure the detail present in the dataset, or cause small random fluctuations in the data to appear significant. Care must be taken to select appropriate values to ensure that the resulting compositional profile is reflective of real changes in chemistry.

In more complicated alloys where many more phases or precipitates are present, the challenges can be even more complex. Different size precipitates can have varying interfacial chemistries that may be missed if all the precipitates are analysed together. Sometimes the chemistry on the outside of a precipitate can vary due to the presence of smaller phases, which can skew a proxigram to give an incorrect average of several interfacial profiles. Meanwhile, peak overlaps between elements in the mass spectrum can also cause incorrect quantification, especially when the two overlapping elements are located in different regions of the material. Understanding some of these potential pitfalls can help to ensure that using APT gives appropriate conclusions that can further the understanding of the microstructure of many materials and applications.

There is not a single set of parameters that will fit each and every single analysis. Parameters need to be adjusted for each material and sometimes for each dataset. This has been emphasised for reconstruction parameters in several occasions over the years, but maybe not as much for data treatment. The limited extent of information available in commercial software packages combined with a lack of transparency in the literature make it very difficult to

understand the influence and hence importance of an appropriate set of parameters. The goal herein has been to highlight some critical aspects that should be considered carefully when treating and interpreting atom probe data.

Acknowledgments

Professor Dave Rugg of Rolls Royce and TIMET are thanked for supplying the Ti 6-4 material. The Focused Ion Beam instruments at Imperial College and Durham were used for the preparation of the titanium and steel samples respectively.

References

1. T. Kelly and D. Larson, 'Atom Probe Tomography 2012', *Annu. Rev. Mater. Res.*, 2012, **42,** 1–31

2. D. Rugg, 'Materials for future gas turbine applications', *Mater. Sci. Tech,* 2014, **30,** 1848-1852

3. B. Gault, F. Vurpillot, A. Vella, M. Gilbert, A. Menand, D. Blavette and B. Deconihout, 'Design of a femtosecond laser assisted tomographic atom probe', *Rev. Sci. Instrum.*, 2006, **77,** 043705

4. J. Bunton, D. Lenz, J. Olson, K. Thompson, R. Ulfig, D. Larson and T. Kelly, 'Instrumentation Developments in Atom Probe Tomography: Applications in Semiconductor Research', *Microsc. Microanal.*, 2006, **12,** 1730

5. R. R. Boyer, 'An overview on the use of titanium in the aerospace industry', *Mater. Sci. Eng.: A,* 1996, **213,** 103–114

6. G. Lütjering and J. C. Williams, 'Titanium', 2003, Verlag New York, Springer

7. R. R. Boyer, 'Attributes, characteristics, and applications of titanium and its alloys', *JOM*, 2010, **62,** 21–24

8. S. Nag, R. Banerjee, R. Srinivasan, J. Y. Hwang, M. Harper and H. L. Fraser, ' ω-Assisted nucleation and growth of α precipitates in the Ti-5Al-5Mo-5V-3Cr-0.5Fe β titanium alloy', *Acta Mater.*, 2009, **57,** 2136–2147

9. T. Li, D. Kent, G. Sha, M. S. Dargusch and J. M. Cairney, 'The mechanism of ω-assisted α phase formation in near β-Ti alloys', *Scr. Mater.*, 2015, **104,** 75–78

10. T. Li, D. Kent, G. Sha, M. S. Dargusch and J. M. Cairney, 'Precipitation of the ??-phase in an ultrafine grained beta-titanium alloy processed by severe plastic deformation', *Mater. Sci. Eng. A*, 2014, **605,** 144–150

11. J. Coakley, V. A. Vorontsov, N. G. Jones, A. Radecka, P.A. J. Bagot, K. C. Littrell, R. K. Heenan, F. Hu, A. P. Magyar, D. C. Bell and D. Dye, 'Precipitation processes in the Beta-Titanium alloy Ti–5Al–5Mo–5V–3Cr', *J. Alloys Compd.*, 2015, **646,** 946–953

12. D. Rugg, T. B. Britton, J. Gong, A. J. Wilkinson and P. A. J. Bagot, 'In-service materials support for safety critical applications – A case study of a high strength Ti-alloy using advanced experimental and modelling techniques', *Mater. Sci. Eng. A*, 2014, **599,** 166–173

13. M. Yan, M. S. Dargusch, T. Ebel and M. Qian, 'A transmission electron microscopy and three-dimensional atom probe study of the oxygen-induced fine microstructural features in as-sintered Ti-6Al-4V and their impacts on ductility', *Acta Mater.*, 2014, **68,** 196–206

14. A. Barrow, H. Bhadeshia, M. Rawson and P. Hill, 'An Alloy Steel', Rolls Royce plc report, 2012

15. O. Dmitrieva, D. Ponge, G. Inden, J. Millán, P. Choi, J. Sietsma and D. Raabe, 'Chemical gradients across phase boundaries between martensite and austenite in steel studied by atom probe tomography and simulation', *Acta Mater.*, 2011, **59,** 364–374

16. D. Raabe, D. Ponge, O. Dmitrieva and B. Sander, 'Nanoprecipitate-hardened 1.5 GPa steels with unexpected high ductility', *Scr. Mater.*, 2009, **60,** 1141–1144

17. E. V. Pereloma, a. Shekhter, M. K. Miller and S. P. Ringer, 'Ageing behaviour of an Fe-20Ni-1.8Mn-1.6Ti-0.59Al (wt%) maraging alloy: Clustering, precipitation and hardening', *Acta Mater.*, 2004, **52,** 5589–5602

18. J. M. Cairney, K. Rajan, D. Haley, B. Gault, P. a. J. Bagot, P.-P. Choi, P. J. Felfer, S. P. Ringer, R. K. W. Marceau and M. P. Moody, 'Mining information from atom probe data', *Ultramicroscopy*, 2015, 1–14 doi:10.1016/j.ultramic.2015.05.006

19. S. Srinivasan, K. Kaluskar, S. Dumpala, S. Broderick and K. Rajan, 'Automated voxelization of 3D atom probe data through kernel density estimation', *Ultramicroscopy*, 2015, **2,** 1–6

20. K. Thompson, D. Lawrence, D. J. Larson, J. D. Olson, T. F. Kelly and B. Gorman, 'In situ site-specific specimen preparation for atom probe tomography', *Ultramicroscopy*, 2007, **107,** 131–139

21. M. K. Miller, K. F. Russell, K. Thompson, R. Alvis and D. J. Larson, 'Review of atom probe FIB-based specimen preparation methods.', *Microsc. Microanal. Off. J. Microsc. Soc. Am. Microbeam Anal. Soc. Microsc. Soc. Canada*, 2007, **13,** 428–436

22. K. Thompson, B. Gorman, D. Larson, B. Van Leer and L. Hong, 'Minimization of Ga Induced FIB Damage Using Low Energy Clean-up', *Microsc. Microanal.*, 2006, **12,** 1736

23. I. J. Polmear, 'Titanium', in *Light alloys* (ed. Polmear, I. J.), 1981, London, Edward Arnold 162–209

24. M. Meisnar, M. Moody and S. Lozano-Perez, 'Atom probe tomography of stress corrosion crack tips in SUS316 stainless steels', *Corros. Sci.*, 2015, **98,** 661–671

25. S. Lozano-Perez, 'A guide on FIB preparation of samples containing stress corrosion crack tips for TEM and atom-probe analysis', *Micron*, 2008, **39,** 320–328

26. D. Larson, T. Prosa, R.M. Ulfig, B.P. Geiser and T. Kelly, *Local Electrode Atom Probe Tomography - A user's guide*, 2013, Verlag New York, Springer

27. B. Gault, M. P. Moody, J. M. Cairney and S. P. Ringer, *Atom Probe Microscopy*, 2012, Springer Series in Materials Science, **160,** Verlag New York, Springer

28. O. C. Hellman, J. B. Du Rivage and D. N. Seidman, 'Efficient sampling for three-dimensional atom probe microscopy data', *Ultramicroscopy*, 2003, **95,** 199–205

29. O. C. Hellman, J. A. Vandenbroucke, J. Rüsing, D. Isheim and D. N. Seidman, 'Analysis of three-dimensional atom-probe data by the proximity histogram', *Microsc. Microanal.*, 2000, **6,** 437–444

30. L. T. Stephenson, M. P. Moody, B. Gault and S. P. Ringer, 'Nearest neighbour diagnostic statistics on the accuracy of APT solute cluster characterisation', *Philos. Mag.*, 2013, **93,** 975–989

31. M. Knop, P. Mulvey, F. Ismail, A. Radecka, K. M. Rahman, T. C. Lindley, B. A. Shollock, M. C. Hardy, M. P. Moody, T. L. Martin, P. A. J. Bagot and D. Dye, 'A New Polycrystalline Co-Ni Superalloy', *JOM*, 2014, **66,** 2495–2501

32. Y. R. Wen, Y. P. Li, a. Hirata, Y. Zhang, T. Fujita, T. Furuhara, C. T. Liu, a. Chiba and M. W. Chen, 'Synergistic alloying effect on microstructural evolution and mechanical properties of Cu precipitation-strengthened ferritic alloys', *Acta Mater.*, 2013, **61,** 7726–7740

33. A. J. London, S. Lozano-Perez, M. P. Moody, S. Amirthapandian, B. K. Panigrahi, C. S. Sundar and C. R. M. Grovenor, 'Quantification of oxide particle composition in model

oxide dispersion strengthened steel alloys', *Ultramicroscopy*, 2015, 1–8
doi:10.1016/j.ultramic.2015.02.013